Chemical Engineering Science 79 (2012) 163–176

Contents lists available at SciVerse ScienceDirect

Chemical Engineering Science

journal homepage: www.elsevier.com/locate/ces

Effect of geometry on the mechanisms for off-bottom solids suspension in a stirred tank

Inci Ayranci [a,*], Márcio B. Machado [a], Adam M. Madej [b], Jos J. Derksen [a], David S. Nobes [b], Suzanne M. Kresta [a]

[a] Department of Chemical and Materials Engineering, University of Alberta, Edmonton, Alberta, Canada T6G 2V4
[b] Department of Mechanical Engineering, University of Alberta, Edmonton, Alberta, Canada T6G 2G8

GRAPHICAL ABSTRACT

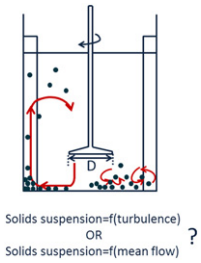

HIGHLIGHTS

- Some combination of mean flow and turbulent eddies provides solids suspension in stirred tanks.
- The solids suspension mechanism changes when the impeller geometry is changed.
- For a $T/3$ impeller the dominant mechanism is the turbulence. For a $T/2$ impeller, neither the turbulence nor the mean flow dominates, but both play a role.
- The $T/3$ impeller is more energy efficient, possibly because a single mechanism dominates.

ARTICLE INFO

Article history:
Received 23 January 2012
Received in revised form
28 April 2012
Accepted 18 May 2012
Available online 30 May 2012

Keywords:
Solids suspension mechanisms
Multiphase flow
Turbulence
Mean flow
Impeller diameter
Mixing

ABSTRACT

This paper probes solids suspension mechanisms in stirred tanks. The hypothesis is that at the point where solids are just suspended a critical flow condition exists close to the bottom of the tank for a fixed solids content and similar geometries. The critical flow condition may be dominated by the turbulence or by the mean flow. Two Lightnin A310 impellers with diameters of $D=T/3$ and $D=T/2$ were tested at varying off-bottom clearances. The mean and the turbulent fluctuating velocities close to the bottom of the tank were determined using both PIV and LES. The results showed that the mechanism of solids suspension is different for the two impeller diameters. Turbulence is the dominant mechanism for the $T/3$ impeller. For the $T/2$ impeller some combination of turbulence and mean flow is required. A comparison between the two impeller diameters in terms of power consumption suggests that solids suspension is more efficient when the turbulence mechanism dominates.

1. Introduction

Complete off-bottom suspension is the most common process requirement for solid–liquid mixing. The impeller speed at this condition is called the just suspended speed (N_{js}), and is defined as the impeller speed at which no particles remain stationary at the bottom of the tank for more than one or two seconds (Zwietering, 1958). Using this criterion Zwietering proposed a correlation for N_{js}:

$$N_{js} = S\left(\frac{g(\rho_S-\rho_L)}{\rho_L}\right)^{0.45} \frac{X^{0.13} d_p^{0.2} \nu^{0.1}}{D^{0.85}} \quad (1)$$

Many later papers provided measurements and tested other correlations for N_{js} (Nienow, 1968; Baldi et al., 1978; Armenante et al., 1998), but the Zwietering correlation is still the most widely

* Correspondence to: Department of Chemical and Materials Engineering, University of Alberta, 7th Floor ECERF, 9107-116 Street, Edmonton, Alberta, Canada T6G 2V4. Tel.: +1 780 492 9221; fax: +1 780 492 2881.
E-mail address: iayranci@ualberta.ca (I. Ayranci).

0009-2509/$ - see front matter © 2012 Elsevier Ltd. All rights reserved.
http://dx.doi.org/10.1016/j.ces.2012.05.028

accepted form for design. There are a number of valid criticisms of this correlation:

- The Zwietering constant, S, varies with impeller type, impeller diameter, off-bottom clearance, the shape of the tank bottom, the baffle geometry, and the particle type.
- The effect of viscosity is questionable since the original experiments did not use a wide range of viscosities.
- When there is only one particle, N_{js} drops to zero, which is non-physical.
- The correlation is only applicable to low solids loadings (<10 wt%) and unimodal slurries.

In addition to the issues listed above, Grenville et al. (2010) showed that S changes on scale-up.

The Zwietering correlation does not successfully predict either the effect of geometry or scale. When the geometry is kept constant and the tank is scaled up, $D^{0.85}$ does not fully capture the effect of scale and S changes. When the scale is kept constant and D changes, S must also change. In order to make progress, a better understanding of the mechanism of solids suspension is required. Since the definition of complete off-bottom suspension is based on conditions at the bottom of the tank, it is not surprising that the impeller diameter alone does not provide enough information. Additional variables such as power number and the off-bottom clearance of the impeller provide more information, but they are not necessarily good predictors of the critical flow condition at the bottom of the tank. To make progress, more information is needed about the critical conditions at the bottom of the tank at the just suspended point and how the tank geometry affects solids suspension.

Baldi et al. (1978) suggested that turbulent eddies are the cause of solids suspension in a stirred tank. Eddies have a range of sizes and energies. Eddies that are close to the particle size are most likely to suspend the particles. This is often generalized to the idea that more solids can be suspended if there is more turbulence or the idea that constant power per volume is a reasonable scale-up rule. Both of these statements are flawed. To illustrate the problem consider two impellers: the Rushton turbine and the A310 impeller. The Rushton turbine is a radial impeller which provides intense turbulence, and the A310 is an axial impeller which provides mostly flow (Zhou and Kresta, 1996). The A310, however, is known to be better for solids suspension with a much lower P_{js} than the Rushton turbine (Ayranci and Kresta, 2011). There are two reasons for the failure of the Rushton turbine in suspending solids. First is the location of the turbulence. The Rushton turbine generates turbulence around the impeller, not at the tank bottom. The A310 directs all of the turbulence it generates towards the bottom. Second is the direction of the flow. The Rushton turbine discharges the fluid radially towards the walls where it divides into two circulation loops one above and one below the impeller. The loop below the Rushton turbine reaches the tank bottom and flows towards the center of the tank where the particles tend to drop out with no means of resuspension. The discharge of the A310 goes directly to the tank bottom and then turns outwards towards the walls. Once it reaches the walls, the baffles direct the fluid and solids upwards, making the solids suspension more efficient.

Next consider two tanks, both with A310 impellers, but different shapes of tank bottom: one has a flat bottom and one has a dished bottom. With the flat bottomed tank, the last point of suspension is at the tank walls, as described above, while with a dished bottom it is in the center. If the baffles are profiled to fit close to the tank bottom in the dished tank, N_{js} is much higher than if they are left as rectangular baffles (Myers and Fasano, 1992). The just suspended speed is clearly sensitive to both the overall flow patterns and the details of the flow close to the bottom of the tank.

Important outcomes of these examples can be summarized as:

- N_{js} depends on the conditions at the bottom of the tank.
- Changing the impeller geometry completely changes the bottom conditions.
- Details of the flow close to the bottom can make a large difference to N_{js}.

These outcomes highlight an important point also emphasized by Thorpe and Stevenson (2003): if the turbulence is not sufficient for solids suspension and other parameters such as the flow pattern have an effect, then some mechanism in addition to turbulence must also play a role in solids suspension.

The hypothesis is further developed using an example with a much simpler geometry. First, the turbulent velocity is broken into two components: the mean velocity and the root mean square of the turbulent fluctuating velocity. Some combination of the velocity components provides the required conditions for solids suspension. To form a better hypothesis of which mechanisms might determine the solids suspension condition, the contribution from each of these velocity components should be well understood.

Consider flow over a smooth flat plate with a single particle. When the particle is sitting on the plate as shown in Fig. 1a the forces acting on the particle are gravity (F_G), buoyancy (F_B), drag (F_D), and lift (F_L). The effect of friction on a rough surface is discussed later in the paper. In Fig. 1b the mean flow on the particle is isolated from the turbulence. The mean flow needs to go over the sphere. This imposes both boundary layer and form drag on the particle and it starts to roll or slide along the plate.

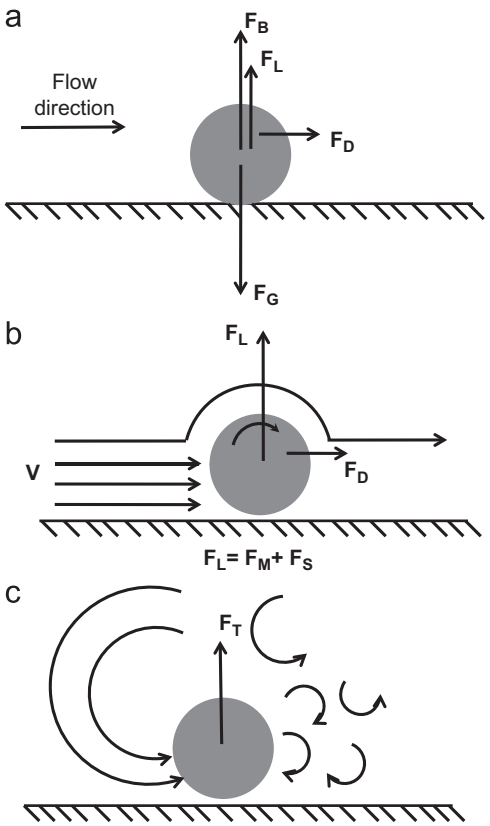

Fig. 1. Effect of mean velocity and turbulence on a particle on a flat plate. (a) The forces effective on the particle. (b) Mean velocity isolated from turbulence. (c) Turbulent eddies isolated from the mean flow.

A pressure difference will develop between the top and bottom of the particle due to the asymmetry of the flow. The pressure difference applies a lift force on the particle. If $F_L > F_G$, the particle lifts off the plate. The lift forces that are caused by the shear and rotation of the particle are known as the Saffman force, F_S, and the Magnus force, F_M, respectively. In Fig. 1c the turbulence is isolated from the mean flow. The eddies formed in a turbulent flow have different energies and sizes. The smallest eddies will not affect the particle. The largest eddies have a convective effect and will act similarly to the mean flow. A range of intermediate sized eddies will have sufficient energy to suspend the particle when they hit it, and will also have a size that is similar to the particle size (Baldi et al., 1978). This is shown as the turbulence force, F_T in Fig. 1c. In this simple case, illustrated with a single particle on a flat plate, both the mean flow and the turbulence can play a role in suspending the sphere.

In a stirred tank with an axial impeller, the solids are carried towards the walls by the mean radial velocity where they meet baffles and the associated vertical wall jets which work as elevators for the particles at the tank walls (Bittorf and Kresta, 2003). The particles that are carried towards the walls are easier to suspend and circulate in the tank, which explains the importance of selecting an axial flow impeller for solids suspension. At the same time as the mean radial velocity convects particles toward the walls, the axial component of fluctuating velocity lifts the particles off the bottom of the tank and into the strong circulating flow. In a hypothetical case where only turbulence is present in the tank without any mean flow, the turbulent eddies can suspend the particles; however, this is a short term suspension since the particles are suspended only slightly from the bottom by the intermediate sized eddies. Each particle settles quickly and is resuspended at some later time, failing on average to lift all particles from the bottom of the tank. Since there is no mean flow the particles are not carried towards the walls and they are not circulated throughout the tank.

Now consider a second hypothetical case where there is only mean flow and no turbulence. The particles are easily carried towards the walls. They are slightly lifted as a result of the combination of drag and lift forces; however, this does not provide complete suspension at the bottom. The particles pile up at the periphery of the tank in low velocity regions. At the walls the radial mean flow is redirected into axial mean flow. This suspends many particles that are at the top layer of the pile; however, a significant fraction of the particles remain stationary at the periphery since there is no turbulence to push them up and out of the stagnant zone they are in. These thought experiments suggest that the complete off bottom suspension condition in a stirred tank could easily require contributions from both velocity components.

Solids suspension has been extensively studied in two other research areas: slurry pipeline flow and river sediment transport. In both flows, the effects of mean flow, turbulence, and near wall lift have been considered. These results are considered next and their applicability to stirred tanks is discussed.

Thorpe and Stevenson (2003) compared solids suspension in stirred tanks and slurry pipeline flow in terms of the definition of suspension and the form of the correlations. The deposition velocity, the minimum solid transport rate below which the particles start accumulating at the pipe wall, is analogous to N_{js} in stirred tanks. The main mechanisms for solids suspension in slurry pipelines are turbulent diffusivity (fluctuating velocity) and near wall lift. In the core region turbulent diffusion provides solids suspension. Near the wall, the turbulence is diminished in the viscous sub-layer. In the horizontal plane close to the viscous sub-layer there is a downwards flux of particles; however, there is no upward flux of particles caused by the turbulence since it is not effective in the viscous sub-layer. In this sub-layer, the balance of the flux of particles is supported by another mechanism which is the near wall lift (Wilson, 2005). This is where the Saffman and Magnus forces become important vertical forces. Recently, Wilson et al. (2010) reported the importance of the ratio of the particle size to the thickness of the viscous sub-layer. When the particle size is small the particles are submerged in the viscous sub-layer. For larger particles, no particles remain in the viscous sub-layer. The thickness of the viscous sub-layer changes according to the mean flow. Higher mean flow results in a thinner viscous sub-layer. This affects the importance of near wall lift, since the ratio of the particle size to viscous sub-layer thickness changes. Turbulence, near wall lift, and the mean flow are all active in providing solids suspension for slurry pipeline flows.

Molerus and Latzel (1987) reported boundary layer effects in stirred tanks. Based on the wall friction on pipeline flow they related a shear Reynolds number for the boundary layer to the Archimedes number (Ar), and defined limits on Ar to determine whether the particle is submerged in the viscous sub-layer.

$$\mathrm{Ar} = \frac{g(\rho_s - \rho_L)d_p^3}{\nu^2 \rho_L} \tag{2}$$

Molerus and Latzel showed that the particles are submerged in the viscous sub-layer if $\mathrm{Ar} < 40$. Larger particles extend beyond the viscous sub-layer, and therefore, different mechanisms apply for these particles. It seems that the Ar does not include a velocity term. The thickness of the viscous sub-layer, however, decreases with an increase in velocity. To test the validity of the argument of a limit on Ar to determine the position of the particle with respect to the viscous sub-layer the details of the Ar should be analyzed. Ar is the ratio of gravitational forces to viscous forces.

$$\mathrm{Ar} = \frac{(\rho_s - \rho_L)g d_p}{\mu_L U/x} \tag{3}$$

The velocity, U, is present in this initial form of the Ar, but not in the final form, so it cancels out in the derivation. Since the focus is on the viscous sub-layer, the length scale, x, can be assumed to be the thickness of the viscous sub-layer, δ, and the velocity, U, becomes U^*, the shear velocity. If $\delta \geq d_p$, then the particle is submerged in the viscous sub-layer. The limiting point is when $\delta = d_p$. Applying this limit and the assumptions to Eq. (3) gives

$$\mathrm{Ar} = \frac{(\rho_s - \rho_L)g d_p}{(\mu_L U^*)/d_p} \tag{4}$$

The U^* is still present in the equation. In slurry pipeline flow a dimensionless particle diameter, d^+ is used to determine whether the particle is submerged in the viscous sub-layer (Wilson et al., 2010).

$$d^+ = \frac{\rho_L d_p U^*}{\mu_L} \tag{5}$$

If $d^+ < 9$, then the particle is completely submerged in the viscous sub-layer, and if $d^+ > 27$, then the particle is significantly larger than the viscous sub-layer and starts to protrude into the logarithmic layer. The near wall lift applies when $9 < d^+ < 27$. This is a limit given for the slurry pipeline transport. Since d^+ is dimensionless, it can be interpreted as some ratio of the particle diameter to δ. In general, for flow close to a solid surface it is known that the viscous sub-layer is located at $y^+ \leq 5$ (Davies, 1972):

$$y^+ = y\frac{U^*}{\nu} \tag{6}$$

When $y^+ = 5$, $y = \delta$. Applying these boundary conditions in Eq. (6) gives

$$\delta = 5\frac{\nu}{U^*} \tag{7}$$

To combine this back to the particle size remember that the particle is submerged in the viscous sub-layer when $d_p=\delta$, and based on Eq. (7) when $d_p=5(\nu/U^*)$. Substituting this information in Eq. (5) shows that $d^+=5$ when the particle is the same size as the viscous sub-layer. Since the limiting d^+ is known, 5, it can be substituted in Eq. (5) to obtain an expression for U^*.

$$U^*=5(\mu_L/\rho_L d_p) \tag{8}$$

When this U^* is replaced in Eq. (4), the final form of the Ar, given in Eq. (2), is obtained with a constant. This scaling argument shows that the limit on the Ar does include the effect of velocity on the thickness of the viscous sub-layer for the fixed condition of particles being submerged in the viscous sub-layer.

The limit based on d^+ can be improved with different assumptions. Further investigation of the Ar criterion and d^+ showed that they can be linked. The Ar is based on the particle shear Reynolds number, and d^+ is the same as the particle shear Reynolds number. Combining the two cases the relation between Ar and d^+ is:

$$d^+=\sqrt{\frac{2}{3}\mathrm{Ar}} \tag{9}$$

This relation applies only for the cases where $\delta=d_p$. The particles are submerged in the viscous sub-layer when $\mathrm{Ar}<40$. This corresponds to $d^+<5$. Note that this limit is the same as the limit based on flow close to a solid surface. There is no limit for stirred tanks at which the particles protrude into the logarithmic layer. For slurry pipelines this limit is $d^+>27$. This limit can loosely be used for the stirred tanks: particle is exposed to near wall lift when $5<d^+<27$, and it protrudes into the logarithmic layer when $d^+>27$. An exact quantitative upper limit cannot be given for stirred tanks because of the complexity of boundary layer development at the bottom of a stirred tank.

River sediment transport is another area where solids suspension has been widely discussed. The motion of solids is caused by the mean flow over a bed of sediment. At very low velocities no sediment moves. At higher velocities individual particles start rolling and sliding intermittently along the bed. As the velocity is further increased the drag and lift on the particles increases; some particles start to make short jumps, leave the bed for a short time and return either to come to rest or to continue in motion on the bed and undergo further jumps. If the mean velocity increases slightly, the particles jump more frequently and some of the grains are incorporated into the main body of the flow by the upward components of the turbulence. They may then stay in suspension for appreciable lengths of time (Vanoni, 2006).

The size of the unsuspended sediment particles determines the surface roughness of the bed, which in turn affects the flow velocity distribution and its sediment transport capacity. If the bottom boundary is smooth, turbulence will be suppressed in the viscous sub-layer near the bed and the capacity of turbulence to suspend solids will be dramatically decreased. This is rarely the case in rivers. Most boundaries in alluvial rivers are hydraulically rough; therefore, there is no viscous sub-layer formation. Turbulence becomes the main mechanism in solids suspension from the bed (Garcia, 2008). The effect of bottom roughness on N_{js} in a stirred tank was studied by Ghionzoli et al. (2007). Their study showed that the N_{js} of particles which have a diameter smaller than 10η, where η is the Kolmogoroff length scale, is reduced on a rough bottom while the N_{js} for larger particles stays the same. The bottom roughness determines the turbulent eddy size and allows the turbulence to be the controlling mechanism for solids which are well matched to the defining eddies.

This analysis of related research areas shows that mean flow and turbulence are the main mechanisms for solids suspension. It seems that both of these mechanisms are necessary for solids suspension: either one of them acting alone may not be sufficient to suspend the solids throughout the volume of a stirred tank In some cases one of the mechanisms may dominate. At the larger scale, the mean flow carries the particles towards the walls. In the boundary layer, the velocity gradient due to the mean flow rolls and/or slides the particles and lifts them out of the viscous sub-layer so that they can be carried towards the walls by the bulk flow. At the same time turbulent eddies of a similar size and inertial energy of the particles lift particles for short periods of time, again exposing them to the bulk flow. We hypothesize that both the mean flow and the turbulent eddies are necessary for solids suspension, but if there is sufficient turbulence with the required eddy size, then the eddies will be the main mechanism that suspend the particles. If there is sufficient mean flow, the turbulence will still contribute to solids suspension, but the mean flow will dominate.

To test this hypothesis, experiments were designed to apply gradual changes to the flow field using constant solid species and solids concentration to compare the critical flow conditions at the just suspended speed. The desired changes are small enough to keep the circulation pattern the same, but large enough to observe a difference in the decay of the impeller discharge stream. Varying the off-bottom clearance of an A310 impeller was chosen as the best way to achieve this objective. If convection across the tank bottom (mean flow) is the dominant mechanism for solids suspension, then all of the mean radial velocity profiles, properly scaled to N_{js}, should collapse onto a single profile for all clearances. In this case the turbulent eddies are still necessary, but their contribution is not sufficient to obtain complete off-bottom suspension. If it is the turbulent eddies which dominate, then the axial rms (root mean square) velocity profiles should collapse onto a single profile for all clearances, and the mean flow profiles will most likely be scattered. The dominant mechanism is tested for two impeller diameters.

The analysis of the dominant mechanism requires the analysis of a collapse in the velocity profiles. This collapse is based on the differences between the single phase velocity profiles and the velocity profiles scaled to N_{js}. The analysis can be done by visual inspection and by inspecting the change in standard deviation. Both these analyses are done to test the hypothesis. An additional analysis based on the particle–eddy interactions is also included.

2. Experimental procedures

To test the hypothesis stated above a three-step plan was prepared. First, the N_{js} of four slurries (three at low and one at high solids loading) was measured at varying off-bottom clearances. Second, single phase velocity profiles, the mean radial velocity and the axial fluctuating velocity, were measured using particle image velocimetry (PIV) and calculated with large eddy simulations (LES) over a horizontal plane close to the tank bottom for the same range of geometries. Third, the velocity profiles were scaled to the just suspended condition at every clearance to identify whether a single critical flow condition exists at the bottom of the tank.

2.1. N_{js} experiments

N_{js} was measured as a function of off-bottom clearance in a flat bottomed cylindrical tank with an inner diameter of 0.24 m, shown in Fig. 2. The tank was equipped with four baffles ($W=T/10$). The liquid level in the tank was equal to the tank diameter ($H=T$). Two Lightnin A310 impellers with diameters $D=T/3$ and $D=T/2$ were used. The A310 was chosen for this study because it generates a purely axial flow and is efficient for solids suspension in terms of the power consumption at N_{js}. The off-bottom clearance, C/T, was varied from 0.15 to 0.358 for the $T/3$ impeller, and from 0.125 to 0.333 for the $T/2$ impeller to ensure that the impeller stream

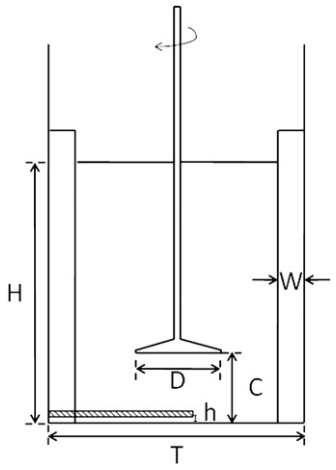

Fig. 2. Cross-section of the cylindrical tank used for N_{js} and PIV experiments, and LES simulations. The dashed plate represents the position of the calibration plate 4 mm above the bottom of the tank. The measurement plane is 3.5–4.5 mm from the bottom of the tank and is 2 mm thick.

Table 1
Specifications of the particles used in the N_{js} experiments.

Type	Density (kg/m^3)	Size (μm)	Ar	Shape
Small glass beads (SG)	2500	74–125	14.7	Spherical
Bronze (B)	8855	150–297	820.5	Spherical
Large glass beads (LG)	2500	595–841	5378.7	Spherical

reached all the way to the tank bottom in all cases. The liquid phase was tap water in all experiments. The cylindrical tank was placed in a square tank in order to minimize the optical distortion, and these two tanks were bolted onto a platform which is open in the middle, in order to leave the bottom of the tank visible from below. More details about the experimental setup and the procedure are given in Ayranci and Kresta (2011).

The just suspended speed, N_{js}, is determined visually by watching the bottom of the tank. N_{js} is the impeller speed at which no particle remains stationary at the bottom of the tank for more than 1 or 2 s (Zwietering, 1958). The impeller speed was increased gradually, and after the system reached steady state (1–2 min) the bottom of the tank was observed. Four slurries were used in the experiments; unimodal slurries of small glass beads (SG), large glass beads (LG), and bronze (B) at low solids loadings and a mixture of small glass beads with bronze at high solids loadings. The specifications of the particles are given in Table 1. The solids loadings of the unimodal slurries of SG, LG and B were 1.5 wt%, and the SG+B mixture loading was 26 wt% SG with 1.3 wt% B. The mixture is at a high solids loading where the presence of particles may start to affect the flow field so the single phase velocity data should be considered with some caution. The data for the B slurry is available only for the $T/3$ impeller, because air entrainment was excessive with the $T/2$ impeller.

2.2. PIV experiments

A stereoscopic PIV system was used to measure velocity profiles close to the tank bottom. The PIV was composed of two high-resolution cameras (14 bit, 2048 × 2048 pixels) which capture images of a seeded flow field illuminated with the double pulse of an Nd:YAG laser (532 nm, 10 Hz, 400 mJ of energy per pulse). The flow facility is a 240 l glass walled holding tank (1200 mm length × 500 mm height × 400 mm width) in which a 240 mm diameter glass cylinder served as the mixing tank. The cameras viewed the region-of-interest from below.

The PIV measurements followed a procedure outlined by Madej et al. (2011). The water in the holding tank was evenly seeded with tracer particles (hollow glass spheres, Potters Industries). The mean particle size of the tracer particles was 11 μm and their specific gravity was 1.1. They were sufficiently small and light to perfectly follow the flow, so the measured particle velocities match the liquid velocity. The light sheet had a thickness of ~2 mm to capture the out-of-plane component of the flow. The stereoscopic PIV system hence resolved the three components of the flow over a 2 mm thick, two dimensional plane. For each operating condition, 2000 image pairs were recorded and the time interval between the two images was set between 700 μs and 1000 μs, depending on the off bottom clearance of the impeller. The lower time interval was used for lower clearances, since the velocities at the bottom were higher when the clearances were lower. The sampling frequency between each image pair was between 1.6 Hz and 2.5 Hz.

In order to determine the camera scaling and the image overlap a target was placed 4 mm above the bottom of the tank. Using the target data the images were dewarped and the camera scaling was calibrated. This allowed the positioning of the 2 mm thick measurement plane 3.5–4.5 mm above the bottom of the tank. Image overlap was further enhanced using a self-calibration of the data to locate the position of the laser sheet as it overlaps with the target. The calibration plate had a diameter of 20 cm and, as shown in Fig. 2, it was positioned such that images can be taken from the center of the tank to the tank wall. Here, only data from the mid-baffle plane is reported.

A three-dimensional cross-correlation PIV algorithm was used to determine the particle displacement over the time interval between the two images. From these displacement vectors, velocity vectors were calculated using commercial software (Davis 7.4, LaVision). The resulting data field is an instantaneous snap-shot of the three components of velocity over the measurement plane. Velocity data processing was carried out using interrogation cell sizes of 64 × 64 pixels for the preliminary step and 32 × 32 pixels with 50% overlap for the final step. At this final interrogation window size, the determined velocity vector is an average over a physical region of 1.116 mm × 1.116 mm in plane by the thickness of the light sheet of ~2 mm.

The glass tank used for the PIV measurements has the same dimensions as the tank used for the N_{js} experiments, with the same ranges of off bottom clearances. Measurements were carried out at a fixed Reynolds number of 48,000.

$$\mathrm{Re} = \frac{\mathrm{ND}^2}{v} \tag{10}$$

A fixed rotational speed was used at all clearances: 200 rpm for the A310 $T/2$ and 450 rpm for the A310 $T/3$ impeller. This avoided shaft vibration and air entrainment at high rotational speeds which would have made the PIV experiments more difficult. The single phase velocities that were measured with PIV are referred to as "measured velocities" throughout the paper. These are the only velocities that were measured. The measured velocities were then scaled to complete off bottom suspension conditions using the N_{js} determined for each off-bottom clearance.

$$V_{scaled} = V_{measured}\frac{N_{js}}{N_{expt}} \tag{11}$$

The N_{js} of the each solid species at each off-bottom clearance was used to scale the measured velocities to the conditions where

solids are present in the tank. These velocities are referred to as "scaled velocities" throughout the paper.

Several authors have shown that velocity profiles below the impeller scale exactly with the tip speed (πND) (Nouri et al., 1987; Zhou and Kresta, 1996). The range of clearances used here falls within a range where this scaling can also be applied at the bottom of the tank (Kresta and Wood, 1993). This was validated through some test experiments.

2.3. LES simulations

A lattice-Boltzmann method was used to discretize the Navier–Stokes equations and a force-field technique was employed to represent the effect of impeller, shaft, baffles and tank wall on the fluid. In the lattice-Boltzmann method, the fluid flow can be considered as a many-particle system where all the particles follow the laws of conservation of mass and momentum (Derksen and Van den Akker, 1999). The particles reside on a uniform cubic lattice. At every time step, particles move to neighboring lattice sites, collide, and exchange momentum.

LES was chosen because of its flexibility in adapting to complex geometries, providing detailed information and using less computer resources compared to direct numerical simulations (DNS). In LES, small scale eddies are filtered out and the large scale eddies are resolved. The effect of the small scale eddies on the large scale is modeled using a subgrid-scale model. For this modeling, the Smagorinsky model with a constant of $c_s=0.1$ was used.

A force-field technique was used to represent the cylindrical tank wall, rectangular baffles, and revolving impeller and shaft in the cubic lattice. These are defined by points on the surface. These points do not need to coincide with the lattice sites. The forces acting on the flow are calculated in such a way that the fluid has prescribed velocities (Derksen and Van den Akker, 1999) at these surface points. Applying the boundary conditions results in the desired curved surface for the tank wall, the rectangular baffles, and the rotating impeller and shaft.

A computational domain with 200^3 grid nodes was used. The Reynolds number was 48,000, which is the same as in the PIV experiments. The simulations were performed for an A310 impeller with a diameter of $D=T/3$ at $C/D=0.45$, 0.675, 0.75, and 0.9. The entire tank was simulated and the three velocity components were computed. The averages were taken for several horizontal planes.

3. Results and discussion

The results are presented in five major sections. First the effect of particle properties, solids loadings and geometry (impeller diameter and off-bottom clearance) on N_{js} are presented. Next the velocity profiles for the $T/3$ and the $T/2$ impellers are evaluated to determine the solids suspension mechanism for each impeller and to examine whether the dominant mechanism depends on the impeller diameter. After the analysis of the experimental data, the hypothesis and the conclusions are compared with the LES results. Finally, the power consumed by the two impellers is compared to better understand the interaction between the observed mechanisms and power consumption.

3.1. N_{js} results

Fig. 3 shows the N_{js} results for the $T/2$ and $T/3$ impellers for unimodal slurries of B, LG and SG at 1.5 wt% and the mixed slurry of 26 wt% SG with 1.3 wt% B, all at varying off-bottom clearances. Within the unimodal slurries the B has the highest density and also the highest N_{js}. The LG and SG have the same density, but LG has a higher N_{js} since it is 7 times larger than the SG. The mixed slurry has the highest solids loading, so it has a higher N_{js} than the LG and the SG, but lower than the B because of particle–particle interactions as explained in Ayranci and Kresta (2011). These trends are consistent for both impeller diameters, and as expected, N_{js} is smaller for the larger impeller diameter. As predicted by the Zwietering equation, an increase in the particle density, particle size or solids loading – in the absence of particle–particle interactions – results in an increase in N_{js}.

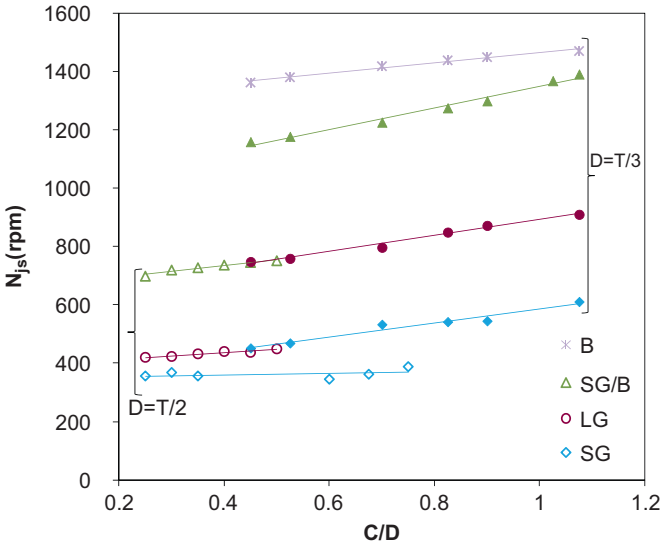

Fig. 3. The effect of impeller diameter, particle diameter, particle density, and solids loading on N_{js}. B, LG and SG are at 1.5 wt% and the mixture of SG+B is at 27 wt% total solids loading with 1.3 wt% B. Solid and hollow symbols represent $D=T/3$ and $D=T/2$, respectively.

The effect of off-bottom clearance on N_{js} is more complex, as shown in Fig. 4. At off-bottom clearances, C/D, larger than 0.35, the particles collect close to the tank walls, and are suspended from there when N_{js} is reached. At off-bottom clearances smaller than 0.35 the particles collect in the center of the tank as well as at the tank walls. This is because the A310 impeller cannot develop purely axial flow below the hub at low C/D and the discharge of the impeller is quickly deflected to produce a swirling radial flow. Fig. 4 shows sample experimental observations of this behavior for a slurry of 1.5 wt% SG with 1.5 wt% B with the $D=T/2$ impeller. At $C/D=0.25$ the particles collect both in the center and at the periphery of the tank, but when the off-bottom clearance is increased to $C/D=0.5$ there is no accumulation in the center: all the particles are at the periphery of the tank. These two deposition patterns will be helpful for understanding some of the later results.

3.2. Solids suspension mechanisms with the T/3 impeller

The evaluation of dominant solids suspension mechanism is based on a hypothesis that the solids suspension occurs as a result of a combination of both mean flow and turbulent eddies, and at the complete off-bottom suspension condition one of these mechanisms, either the turbulence or the mean flow, should dominate for a fixed set of particles. For a purely axial impeller, the flow pattern stays the same as the off-bottom clearance is increased and thus the velocity component which is dominant at the point of off-bottom suspension should also remain the same. If this hypothesis holds, a set of velocity profiles should collapse onto a single curve for all off-bottom clearances when the measured profiles are scaled to N_{js} at the respective clearances.

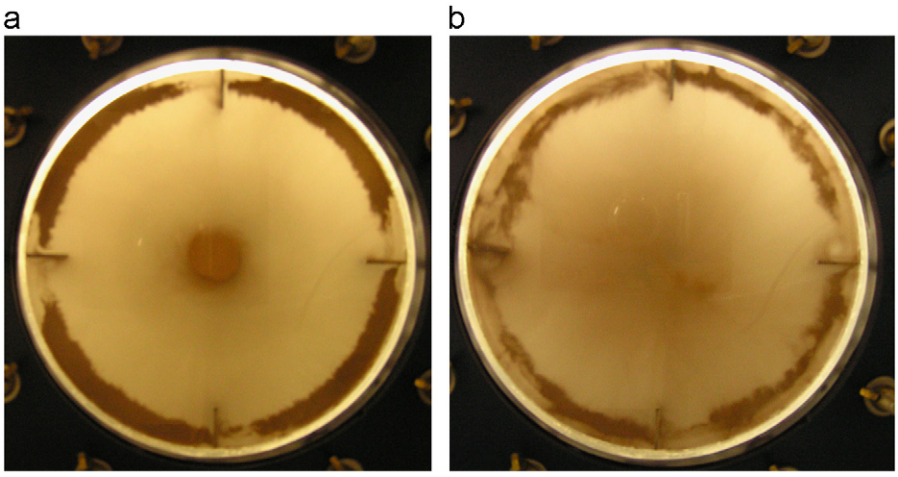

Fig. 4. The effect of off-bottom clearance on the solids suspension pattern for the A310 $D=T/2$. (a) $C/D=0.25$. (b) $C/D=0.5$.

This hypothesis is evaluated based on both the visual inspection of scaled velocity profiles for mean radial velocities, V_r, and axial rms velocities, v'_z, and the reduction in normalized standard deviation for scaled V_r or v'_z over the range of clearances at each point in the profile. A comparison of estimated eddy sizes with particle sizes was also made to further probe the mechanisms. The analysis starts with the measured velocity profiles.

The measured V_r and v'_z at seven off-bottom clearances were normalized with the tip speed of the impeller and are shown in Fig. 5a and b. The profiles in each graph show similar trends for increasing off-bottom clearances, but they do not follow a definite order. In Fig. 5a the V_r profile for the highest clearance, $C/D=1.075$, is 12% lower than the other clearances in the 40–100 mm area. This is because the discharge of the impeller loses a significant amount of momentum by the time it reaches the bottom of the tank when the impeller is more than one impeller diameter away from the tank bottom. While the data for this clearance in the center blends in with the rest, it cannot sustain similar level of velocities in the 40–100 mm area. This clearance was eliminated from the rest of the figures because it violates the basic assumption of having a constant circulation pattern. In Fig. 5a another irregularity is seen for $C/D=0.675$ and $C/D=0.75$ in the 95–120 mm area. While the circulation pattern remains to be the same as the rest of the clearances tested, a transition is seen. The maximum radial velocity can be sustained longer at these off-bottom clearances. In Fig. 5b for these two clearances the position of the peak velocity is slightly shifted, and after 40 mm v'_z is slightly higher than the rest of the data. The remaining profiles for both V_r and the v'_z are quite close to each other at varying off-bottom clearances when normalized with tip speed. This indicates that the expected collapse with either one of the velocity profiles may be difficult to determine by inspection when the profiles are scaled. To allow a more objective assessment, the collapse was also analyzed in terms of $\Delta\sigma$, the point by point difference between the standard deviation of the scaled velocity profiles and the measured velocity profiles for each slurry.

The measured velocity profiles were scaled to N_{js} for four slurries: SG, LG, B, and the mixture of SG with B. For all four slurries the last point of suspension is at the tank walls. The SG slurry results were representative and are reported here. The scaled V_r profiles in Fig. 6a are scattered over most of the profile but collapse from 40 to 65 mm, which is right after the tip of the blade, for all clearances when compared to the measured velocities in Fig. 5a. The scaled v'_z profiles in Fig. 6b are scattered

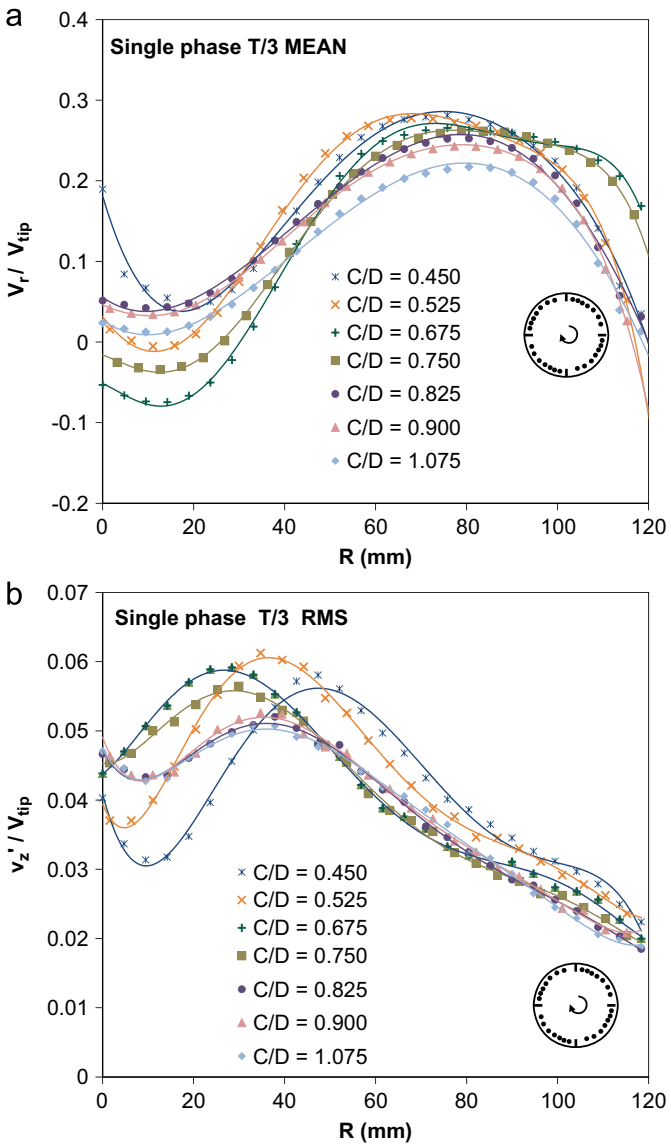

Fig. 5. (a) Measured mean radial velocity profiles normalized with the tip speed of the impeller: A310 $T/3$. (b) Measured axial rms velocity profiles normalized with the tip speed of the impeller: A310 $T/3$.

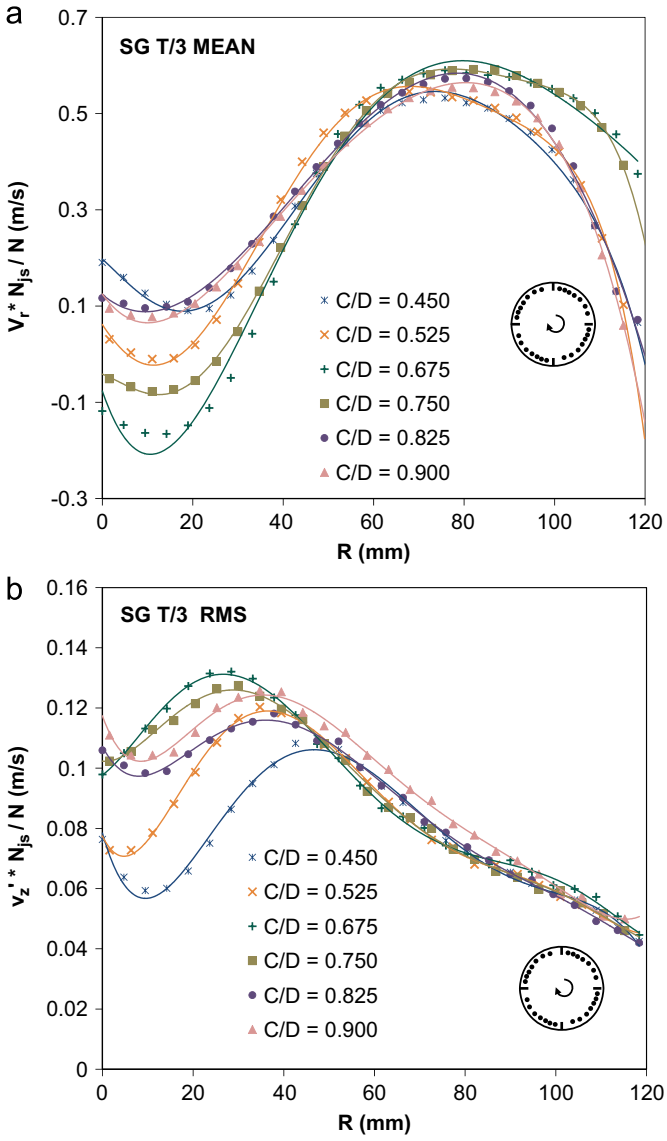

Fig. 6. (a) Scaled mean radial velocity profiles for 1.5 wt% SG with the A310 *T*/3. (b) Scaled axial rms velocity profiles for 1.5 wt% SG with the A310 *T*/3.

over the first 40 mm, which is the area below the impeller blades. From 40 mm to the tank walls the v_z' profiles collapse, and the collapse becomes more significant after 80 mm. The v_z' profiles collapse over most of the radius and the collapse is more significant than the small part in V_r. This shows that some level of mean flow is necessary, but a certain level of turbulence is required for solids suspension. The turbulence is the dominant mechanism for solids suspension with the *T*/3 impeller.

While we categorize some parts of these figures as collapsed, the collapse is not perfect and the measured profiles are quite close to each other for varying clearances, so it is prudent to analyze the data from another perspective to verify that this initial conclusion is correct.

The normalized standard deviation (σ) of the velocities for all six clearances was calculated at each radial position for both velocity components (V_r and v_z').

$$\sigma = \sqrt{\frac{\sum_{n=1}^{n=6}(x_n - x_{mean}/x_{mean})^2}{6-1}} \tag{12}$$

Here n signifies the off-bottom clearance. For each impeller there are six off-bottom clearances. x_n is either V_r or the v_z' at the nth off-bottom clearance, x_{mean} is the mean of the velocities at all off-bottom clearances. This calculation is repeated for every radial position and the difference between the normalized standard deviation of the measured and the scaled results, $\Delta\sigma$, is calculated as:

$$\Delta\sigma = \left[\sqrt{\frac{\sum_{n=1}^{n=6}(x_n - x_{mean}/x_{mean})^2}{6-1}}\right]_{scaled} - \left[\sqrt{\frac{\sum_{n=1}^{n=6}(x_n - x_{mean}/x_{mean})^2}{6-1}}\right]_{measured} \tag{13}$$

The change in normalized standard deviation, $\Delta\sigma$, is reported in Fig. 7a and b for V_r and v_z' and for all four particle species. Values above zero indicate that the profiles are more scattered, and values below zero indicate that profiles have collapsed. The results confirm the conclusions made from Fig. 6. Turbulence is clearly the dominant mechanism for all four slurries for the *T*/3 impeller. The collapse of the mean radial velocity is erratic, actually becoming more scattered in the area immediately below the impeller blades (0–40 mm) where very large or very small

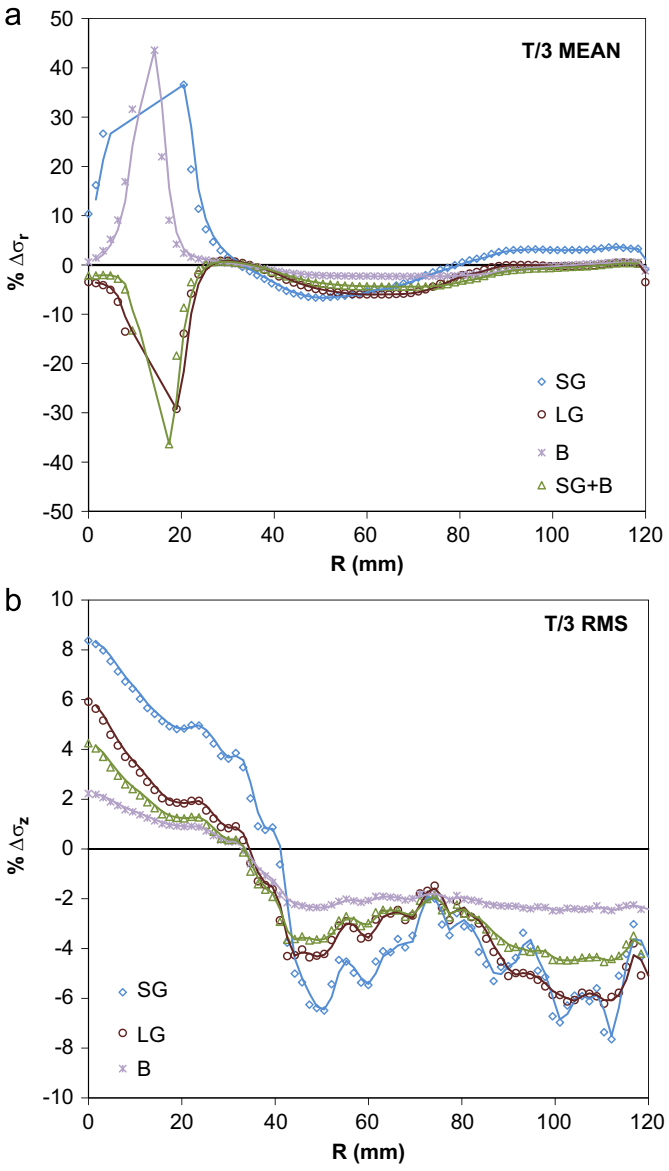

Fig. 7. (a) The difference between the normalized standard deviation of the scaled and the measured mean radial velocity for each particle species with the A310 *T*/3. (b) The difference between the normalized standard deviation of the scaled and the measured axial rms velocity for each particle species with the A310 *T*/3.

$\Delta\sigma$ are seen. This is not surprising because the mean V_r over all clearances is close to zero in this area, and in the $\Delta\sigma$ calculations the velocities are divided by the mean of the velocities. The profiles show more agreement over the middle region (40–80 mm), increasing again from 80–120 mm. This shows that the hypothesis holds true for the $T/3$ impeller: both the mean flow and the turbulent eddies are necessary for solids suspension, but the turbulent eddies dominate. A certain level of turbulence should be reached at the bottom of the tank with the contribution of some mean flow in order to achieve complete off-bottom suspension.

A final analysis was done based on the size of the smallest eddies—the Kolmogoroff length scale (η). A minimum and a maximum η can be estimated at the bottom of the tank using the following scaling arguments. An axial flow impeller generates turbulence at the bottom of the tank, with the smallest eddy sizes, the Kolmogoroff scale, following the relationship:

$$\eta_{est} = \left(\frac{\nu^3}{\varepsilon}\right)^{1/4} \tag{14}$$

where ν is the kinematic viscosity and ε is the energy dissipation. The energy dissipation can be estimated from:

$$\varepsilon = A\frac{\nu_z'^3}{L} \tag{15}$$

where A is 1.0 for isotropic turbulence, ν_z' is the axial rms velocity, and L is the integral length scale. Two integral length scales might be considered: the size of the trailing vortices close to the impeller, $L=D/10$, and the size of the circulation layer at the bottom of the tank, $L=T/5$. Since the trailing vortices are at the impeller, and the eddies get larger towards the bottom of the tank (Tatterson et al., 1980), the length scale at the bottom of the tank should be larger than $D/10$. Similarly, the length scale at the bottom of the tank should be smaller than the circulation layer close to the bottom of the tank, $L<T/5$. Based on these two limiting length scales and the measured ν_z', a maximum and a minimum limit on the Kolmogoroff length scale of the eddies can be estimated:

$$\eta_{min} = \left(\frac{\nu^3}{A(\nu_z'^3/(D/10))}\right)^{1/4} \tag{16}$$

$$\eta_{max} = \left(\frac{\nu^3}{A(\nu_z'^3/(T/5))}\right)^{1/4} \tag{17}$$

The ν_z' in Eqs. (16) and (17) was determined from the scaled velocity profiles for each particle. Over the sections where the profiles collapsed the maximum ν_z' was used in Eq. (16) to estimate η_{min}, and the minimum ν_z' was used in Eq. (17) to estimate η_{max}. Table 2 shows the results. For SG, the range of smallest eddy sizes overlaps the range of particle sizes so the particles are much smaller than the most energetic eddies and will be swept up mainly by turbulent convection from eddies much larger than the particles. For LG, the particles are much larger than the smallest eddies (about 10 ×) but substantially smaller than the integral scale (10–80 ×), so the particle–eddy interaction at the particle scale may be expected to be quite strong. For B, the particles are 3–4 times η, and again the potential for particle–eddy interaction is quite strong.

Table 2
The range of Kolmogoroff length scales for each particle species as observed for two impeller diameters.

Particle type	Impeller diameter	Minimum ν_z' (m/s)	Maximum ν_z' (m/s)	L_{min} (m)	L_{max} (m)	η_{min} (μm)	η_{max} (μm)
SG	$T/3$	0.04	0.10	0.008	0.048	53	165
LG	$T/3$	0.07	0.10			53	115
B	$T/3$	0.10	0.30			23	83
SG	$T/2$	0.10	0.28	0.012	0.048	27	83
LG	$T/2$	0.33	0.10			24	83

3.3. Solids suspension mechanisms with the T/2 impeller

Following the same procedure that was used for the $T/3$ impeller, the collapse of the scaled velocity profiles for the $D=T/2$ A310 was first evaluated visually, and then using $\Delta\sigma$. Fig. 8a and b shows the measured V_r and the ν_z' for six clearances, normalized with the tip speed of the impeller. There are two groups in both figures: a low clearance group, $C/D \leq 0.35$, and a high clearance group, $C/D > 0.35$. In terms of C/D, the clearances in the high-clearance group are comparable to the clearances used for the $T/3$ profiles. In the high clearance group the particles collect around the periphery of the tank, and in the low clearance group the particles settle out in the center of the tank as well as around the periphery. While this initially suggests that the mean radial flow must be small at the center of the tank for low clearances Fig. 8a shows that the normalized mean radial flow is

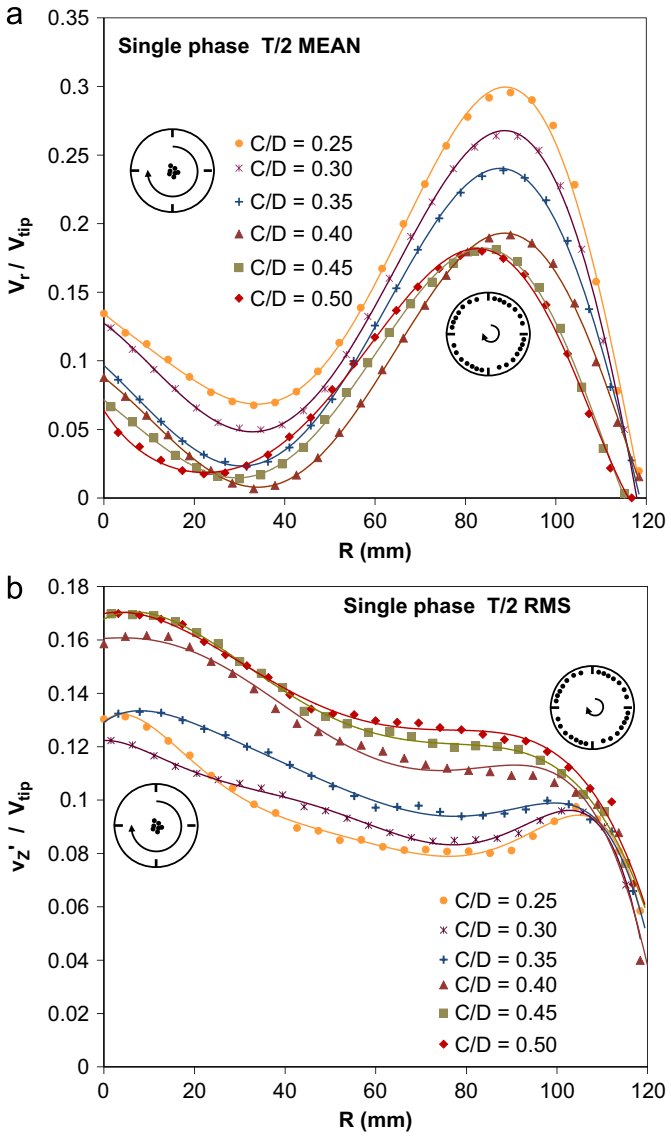

Fig. 8. (a) Measured mean radial velocities normalized with the tip speed of the impeller: A310 $T/2$. (b) Measured axial rms velocities normalized with the tip speed of the impeller: A310 $T/2$.

actually larger than what it is in the high clearance group. Some other effect is dropping particles out in the center of the tank at low clearances.

This additional effect is a strong rotational flow below the impeller. This swirl diminishes when there is sufficient distance between the impeller and the tank bottom, but when the impeller is close to the tank bottom, $C/D \leq 0.35$, the swirl is contained between the impeller and the tank bottom causing particles to drop out. This requires the analysis of the theta velocities. The profiles are not shown here, but an analysis is provided. From 0 to 30 mm along the radial traverse a forced vortex is evident in the theta velocity profiles, followed by a free vortex which extends towards the tank walls. In the 0–30 mm area the theta velocities normalized with the tip speed of the impeller increase up to 0.12 with a steep slope. This high velocity causes the particles drop out in the center immediately below the 20 m diameter hub. As the off-bottom clearance increases, $C/D > 0.35$, the theta velocity drops showing free vortex behavior all along the radius.

The measured velocities were scaled to N_{js} for three slurries: SG, LG, and the mixture of SG with B. For all of the slurries the last point of suspension at low clearances is both at the center of the tank and at the tank walls, and at high clearances it is only at the tank walls. The LG slurry results are representative and are shown in Fig. 9a and b. Visual inspection indicates that with the $T/2$ impeller the contribution of both mean flow and turbulent eddies is necessary, but neither of them dominates. The data does not show any collapse in either the low clearance or the high clearance group. This indicates that the hypothesis does not hold true for the $T/2$ impeller.

The $\Delta\sigma$ results are shown in Fig. 10a and b. $\Delta\sigma$ is always negative for V_r, and is always positive for v_z', suggesting that mean flow is the principle mechanism for the $T/2$ impeller, but this does not agree with the visual inspection of the velocity profiles, which are nearly unchanged. The same conflicting result was observed for LG, SG and the mixture of SG with B.

The two impellers can be directly compared by plotting the velocity profiles for the $T/3$ mean and rms scaled for N_{js} of the LG directly on top of the plots for the $T/2$ impeller. This is shown in Fig. 9a and b as dashed lines. Considering first the mean velocity profiles, the $T/3$ result falls above the two results for the $D=T/2$ impeller at both high and low clearances. The drop in V_r close to the center of the tank is much smaller for the $T/3$ impeller,

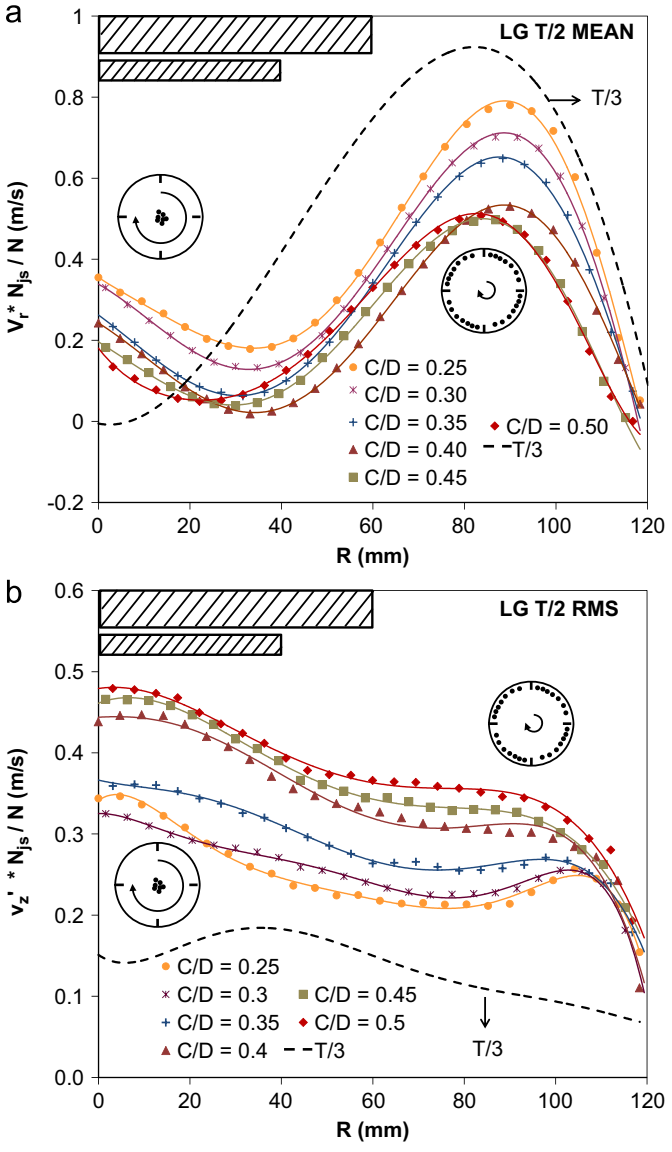

Fig. 9. (a) Scaled mean radial velocity profiles for 1.5 wt% LG with the A310 $T/2$. (b) Scaled axial rms velocity profiles for 1.5 wt% LG with the A310 $T/2$.

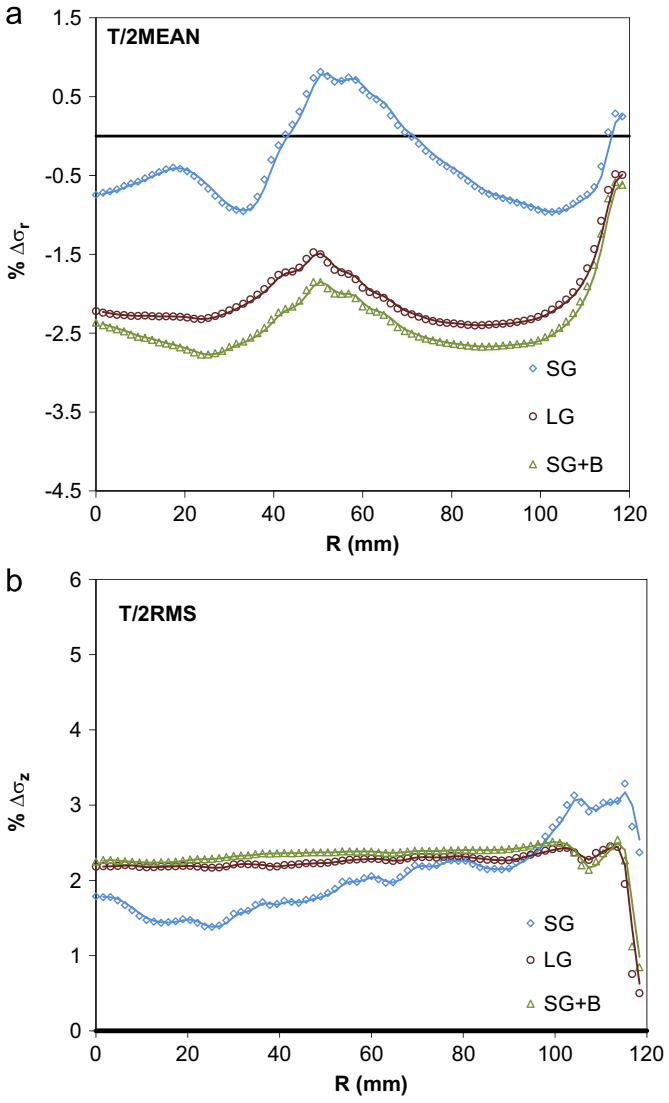

Fig. 10. (a) The difference between the normalized standard deviation of scaled and the measured mean radial velocity profiles for each particle species: A310 $T/2$. (b) The difference between the normalized standard deviation of scaled and the measured axial rms velocity profiles for each particle species: A310 $T/2$.

extending out to only 8 mm, while the $T/2$ impeller retains this trend out to 40 mm. This is a direct effect of the change in impeller diameter. For both impellers, the maximum radial velocity occurs at about 80 mm, but for the $T/2$ impeller this is a sharp peak, while for the $T/3$ impeller, it is a broad peak which extends from roughly 60–100 mm. Again, this is a direct effect of the impeller geometry. The larger impeller has less space to reach the peak, so the slope of the profile on either side must be steeper. Overall, the mean radial velocities are of a similar magnitude, with the $T/2$ impeller having a significantly less favorable configuration for removing solids from the bottom of the tank. The more surprising results are found by comparing the fluctuating velocity profiles. The LG particles can be suspended when the scaled fluctuating velocities are in the 0.8–1.8 range and there is some mean flow present with the $T/3$ impeller. For the $T/2$ impeller, the rms velocity is 3–4 times larger than the required rms velocity. This is because of the shape of the radial velocity profiles with the $T/2$ impeller and proves that the contribution of mean flow is certainly important. In order to achieve the required minimum convective effect with the mean velocity, the $T/2$ impeller generates much more turbulence as a secondary effect.

As a last note, consider the high and low clearance cases. The low clearance case, where particles tend to collect at the center of the tank, has a higher mean velocity and a lower rms velocity in this group. This suggests that some other mechanism is drawing particles into the center of the tank, and the mean velocity has to be increased to compensate for this effect. The rms velocity cannot convect the particles away from the center, so it plays a less critical role for this particular configuration.

An estimation of the size of the smallest Kolmogoroff eddies was also made for the $T/2$ impeller, as given in Table 2. There is no significant collapse of the velocity profiles for this impeller, so the minimum and maximum v'_z were taken close to the tank walls, from 100–120 mm. The SG particles are similar in size to the smallest eddies, while the LG particles fall in the center of the most energetic eddy size range. Note that the maximum Kolmogoroff eddy size is smaller than for the $T/3$ impeller due to the increase in the rms velocity. This will lead to an increase in power consumption with no improvement in solids suspension conditions.

The mean and rms velocity results reveal several things: solids suspension for the $T/3$ impeller is determined by the rms velocity limit, and the profiles collapse nicely to show this. The $T/2$ impeller, on the other hand, is limited by an unfavorable mean radial velocity profile. Overcoming the limitations of this profile requires a significant increase in the rms velocity beyond what is required to suspend the particles. For the low clearance case, some additional three dimensional effect is driving particles toward the center of the tank, and this effect has to be overcome by further increasing the mean velocity. These results show that the solids suspension mechanism changes when the impeller diameter is changed for a fixed set of particles. This is because the flow close to the tank bottom changes, and the particles have to respond to the change in flow.

3.4. LES results

In the final stage of analysis, single phase velocity profiles were obtained using LES at the same conditions as the PIV experiments for the $T/3$ impeller. The advantage of LES is that the flow field in the entire tank is calculated and the data for every grid point is stored. This allows us to investigate the velocity profiles at different horizontal measurement planes. In this section, the critical flow condition hypothesis is tested for a final time using the LES results, and the LES and the PIV results are compared. Second, the sensitivity of the velocities to the position of the measurement plane was analyzed using the high resolution LES data.

3.4.1. Solids suspension mechanisms with the T/3 impeller and comparison of the LES and PIV data

Fig. 11a and b shows the scaled V_r and v'_z for the $T/3$ impeller. Both the V_r and the v'_z profiles are scattered; there is no visible collapse of the profiles. The visual inspection does not show a clear trend for a dominant solids suspension mechanism. Fig. 12a and b shows the $\Delta\sigma$ for V_r and v'_z. The $\Delta\sigma$ for V_r is mostly negative, while the $\Delta\sigma$ for v'_z is negative only from 75 to 105 mm. This suggests that the mean flow is the dominant mechanism for the $T/3$ impeller. The $\Delta\sigma$ analysis leads to a different conclusion than both the visual inspection and the PIV results.

The shapes of the scaled velocity profiles with LES, Fig. 11a and b, are similar to the PIV profiles, Fig. 6a and b, but there are some differences in both the flow details and in the magnitude of the velocities. In Fig. 11a, V_r calculated using LES is zero in the center of the tank while it is between -0.1 and 0.2 m/s in the PIV measurements, giving a mean of zero. In a mathematical sense V_r must approach zero at the bottom center of the tank because

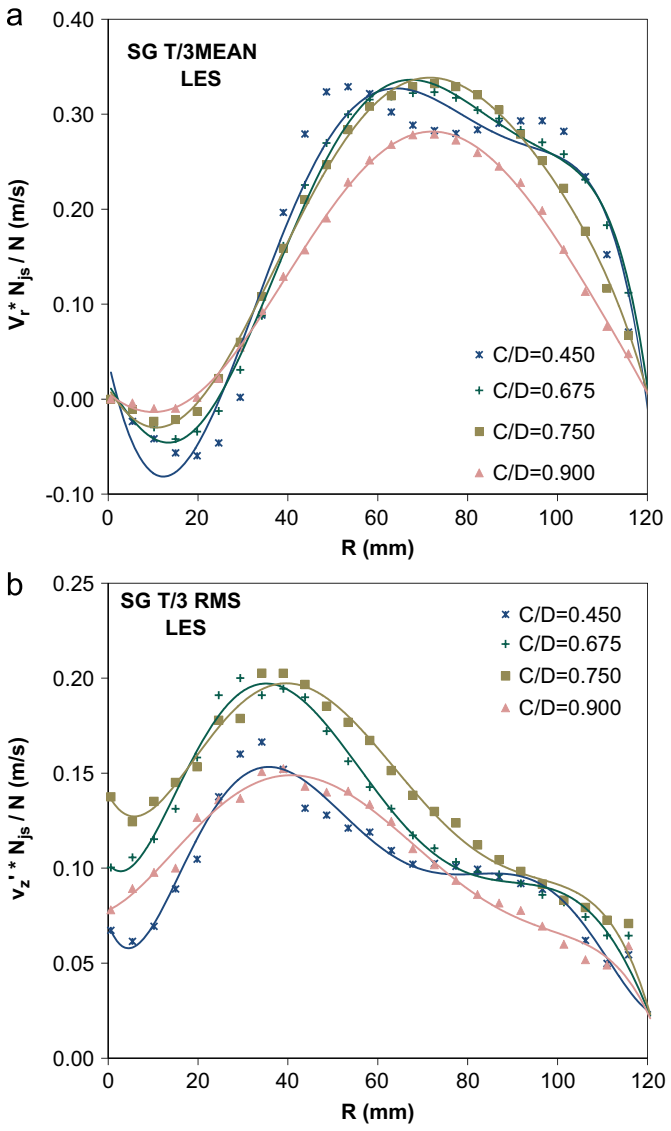

Fig. 11. (a) LES results for the scaled mean radial velocity profiles for 1.5 wt% SG: A310 $T/3$. (b) LES results for the scaled axial rms velocity profiles for 1.5 wt% SG: A310 $T/3$.

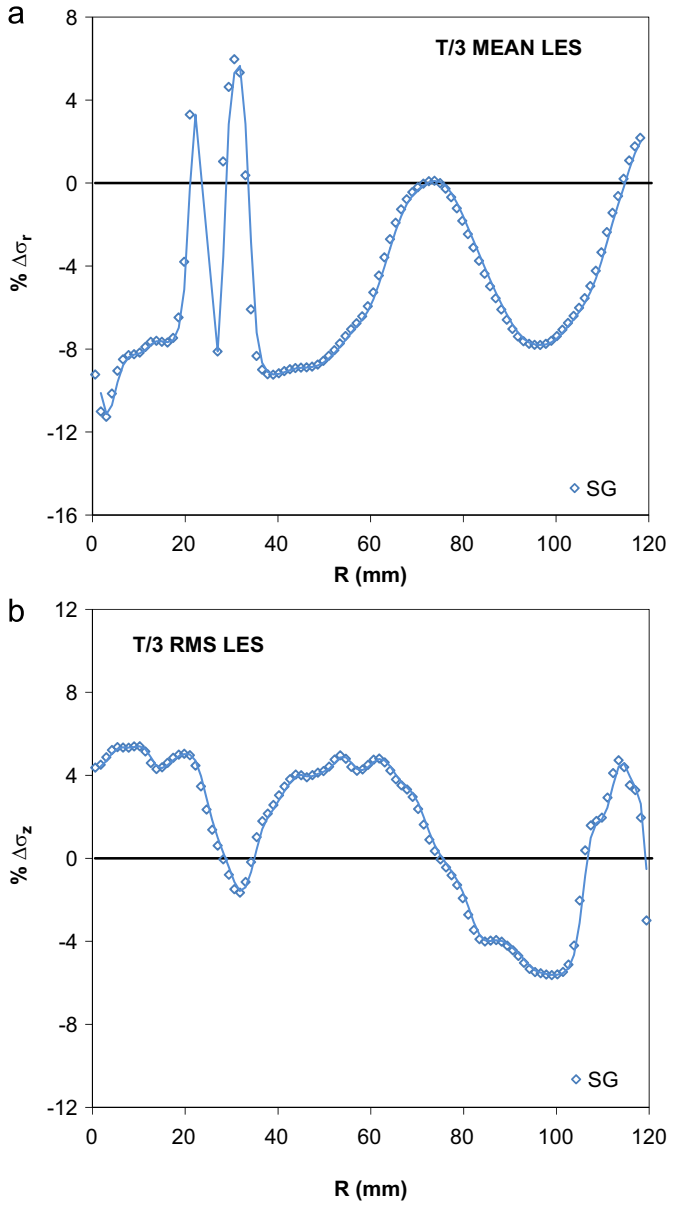

Fig. 12. (a) The difference between the normalized standard deviation of the scaled SG and the single phase mean radial velocities according to LES. (b) The difference between the normalized standard deviation of the scaled SG and the single phase radial mean velocities according to LES.

there is no point source of mass at $R=0$. Capturing an exact zero velocity at the center of the tank would require measurements with a longer time average as well as high resolution in both time and space close to the center of the vessel, and a thoughtful consideration of the best time averaging scheme to apply if a slow precessing vortex structure is present in this region. This detailed flow analysis is beyond the scope of work considered here.

In the LES results, the magnitude of V_r is under-predicted, and the magnitude of v'_z is over-predicted. The LES profiles are located 4.2 mm above the bottom of the tank, which is a region where wall effects may have a substantial impact on the accuracy of LES predictions.

3.4.2. *The effect of distance from the bottom of the tank on velocities*

The LES profiles in Fig. 11a and b were taken 4.2 mm above the bottom of the tank. In the PIV experiments the axial position of the measurement plane was from 3.5 to 4.5 mm above the bottom of the tank, and the thickness of the plane was 2 mm. Close to the bottom of the tank the velocities may vary significantly, so it is interesting to consider how sensitive the results may be to small errors in positioning. This analysis cannot be done with the PIV data since it was only at one vertical position, but LES data was recorded for all horizontal planes along the vertical axis.

Fig. 13a shows the scaled mean radial velocity profiles at a fixed impeller off-bottom clearance, $C/D=0.75$, at various distances from the bottom of the tank. As the plane moves away from the bottom of the tank the radial velocities vary slightly close to the center of the tank and close to the tank walls, but they all collapse on to a single profile at around the maximum V_r.

Fig. 13b shows the scaled axial rms velocity profiles at a fixed off-bottom clearance, $C/D=0.75$, for a $T/3$ impeller. As the plane is pulled away from the bottom of the tank the trend of the profiles remains the same, but the magnitude of the velocities increases. Between the first plane, $i=1.8$ mm, and the second plane,

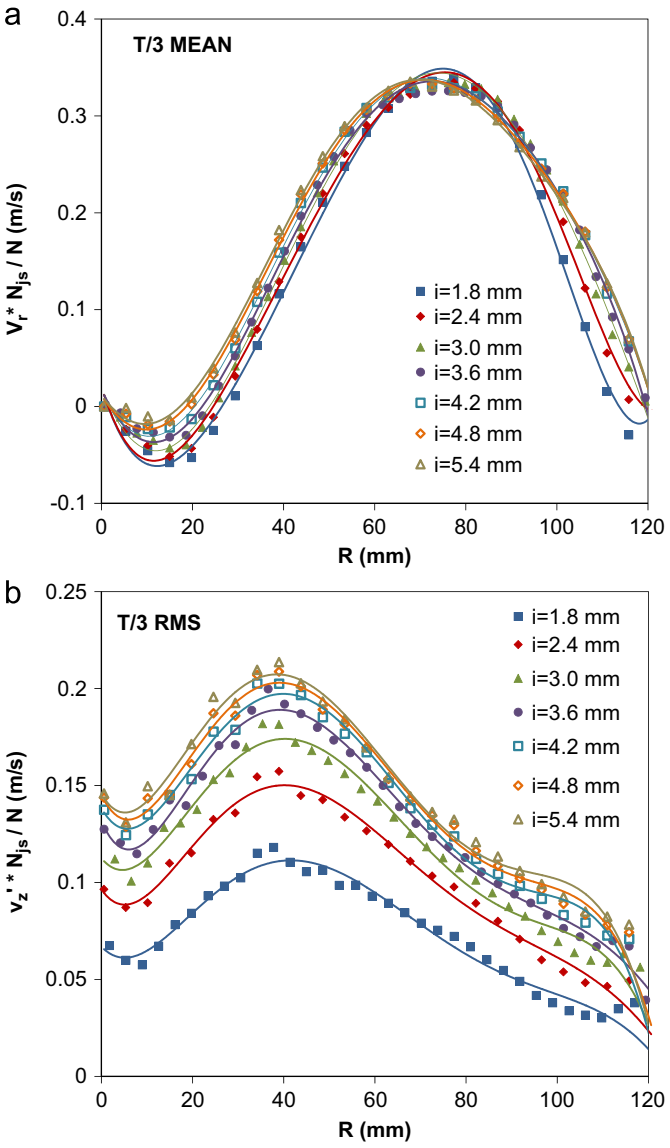

Fig. 13. (a) The effect of the position of the measurement plane on mean radial velocities. Mean radial velocities were obtained with LES and scaled with N_{js} data for 1.5 wt% SG with the A310 $T/3$ at $C/D=0.75$. (b) The effect of the position of the measurement plane on axial rms velocities. Axial rms velocities were obtained with LES and scaled with N_{js} data for 1.5 wt% SG with the A310 $T/3$ at $C/D=0.75$.

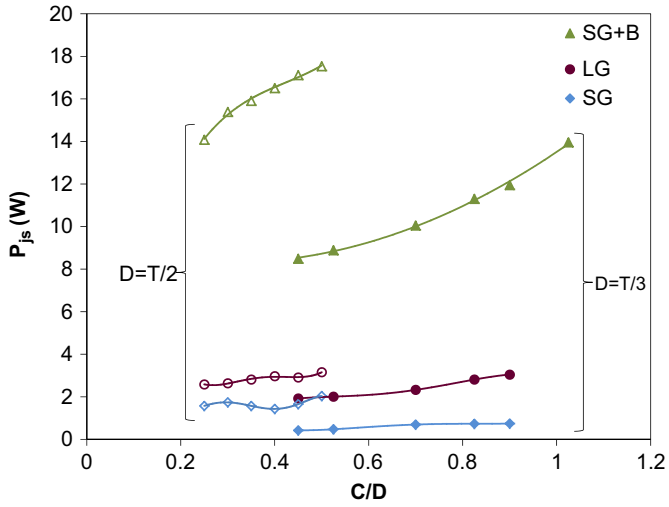

Fig. 14. The comparison of power consumption between the A310 $T/3$ and the $T/2$. The power consumption was calculated for the SG and the LG slurries at 1.5 wt%, and for the mixture at 26 wt% SG with 1.3 wt% B. Solid and hollow symbols represent $D=T/3$ and $D=T/2$, respectively.

$i=2.4$ mm, the magnitude of the velocities increases significantly, showing that the position of the measurement plane makes a significant difference in the velocities. Starting from 3.6 mm the profiles collapse onto each other, indicating that from 3.6 mm to 5.4 mm the axial rms velocities do not change significantly. This analysis shows that the velocities are not a strong function of the position of the measurement plane in the 3.5–4.5 mm range.

3.5. Comparison between the T/3 and the T/2 impellers

Solid–liquid mixing is a power intensive operation; therefore, the power consumption is an important criterion in choosing an impeller. The power consumption at just suspended conditions (P_{js}) can be calculated from:

$$P_{js} = \rho_{sl} N_p N_{js}^3 D^5 \tag{18}$$

Fig. 14 shows the comparison of power consumption between the $T/3$ and the $T/2$ impellers for the SG and the LG slurries at 1.5 wt% and SG+B mixture at 27 wt% at varying off-bottom clearances. For all slurries the power consumption with the $T/3$ impeller is significantly lower than the $T/2$ impeller. Referring back to Fig. 3 we see that N_{js} is higher for the $T/3$ impeller than the $T/2$ impeller for both the SG and the LG slurries. From an operational point of view, the power consumption is a better criterion than N_{js} for choosing an impeller.

A comparison of the two impellers in terms of the solids suspension mechanisms shows two different trends. For the $T/2$ impeller some combination of the mean flow and turbulent eddies provides solids suspension, and neither of these mechanisms dominate. For the $T/3$ impeller a single mechanism, turbulence, dominates and the required level of turbulence with the small impeller is approximately one third the levels observed for the $T/2$ impeller. The $T/3$ impeller is also less power intensive. It can be concluded that the $T/3$ impeller is more efficient because the convective flow is more efficient, which in turn minimizes the amount of turbulence energy dissipation required to suspend the solids.

4. Conclusions

The goal of this study was to investigate the mechanisms that drive solids suspension in stirred tanks. The analysis was based on the hypothesis that at complete off-bottom suspension a critical flow condition exists close to the bottom of the tank at every clearance for fixed solids, tank geometry, and constant circulation pattern. The flow condition might be dominated by either the mean flow in a convective mechanism, or the turbulence in an eddy-lifting mechanism.

Data was collected using visual observations of the tank bottom, PIV, and LES. The PIV measurements were collected at a single rotational speed. The data was analyzed using three separate methods. First the velocity profiles were scaled with N_{js} and plotted together to determine whether the profiles collapsed to a single critical flow condition at N_{js}. Second, the degree of collapse was quantified using the change in normalized standard deviation from the raw measured profiles to the scaled velocity profiles. Last, the size of the smallest eddies was estimated and compared with the size of the particles to determine the most likely type of particle–eddy interactions for each particle species. The results led to the following conclusions:

- Solids suspension occurs as a result of the combination of mean flow and turbulent eddies. Complete off-bottom suspension cannot be obtained in the absence of one of these mechanisms.
- When the impeller diameter is changed the solids suspension mechanism changes. The solids deposition pattern changes when the off-bottom clearance is changed. This data provides two clear demonstrations of the dramatic effect of geometry on solids suspension.
  - For the $T/3$ impeller the hypothesis holds true. The critical flow condition is dominated by the level of turbulence and convection plays a secondary role.
  - For the $T/2$ impeller the hypothesis does not hold true. Both mechanisms play an active role, but neither mechanism dominates. The shape of the radial velocity profile is unfavorable for solids suspension so a larger impeller speed is needed to achieve the same amount of convective flow and this results in a significant amount of additional turbulence and power consumption at the point of solids suspension.
- The solids suspension mechanism also depends on the type of the particle, because the particle–eddy interactions are different for each particle species.
  - The SG is submerged in the viscous sub-layer and it is significantly smaller than the most energetic eddies.
  - The LG lies in the middle of the spectrum with highly energetic particle–eddy interactions all along the tank bottom.
  - The B lies somewhere in between: it is larger than the viscous sub-layer and the smallest eddy sizes, but the particle–eddy interactions are not as strong as for LG. This suggests that the B is moved away from the tank bottom as a result of both turbulent eddies and near wall lift.
- The $T/3$ impeller is more efficient for solids suspension because less energy is lost to excess turbulent energy dissipation.

Nomenclature

Roman characters

A	constant in Eqs. (15)–(17)
C	off-bottom clearance of the impeller (m)
c_s	Smagorinsky model constant
D	impeller diameter (m)
d_p	particle diameter (m)
d^+	particle diameter (dimensionless)
F_B	buoyancy force (N)

F_D	drag force on the sphere (N)
F_G	gravity force (N)
F_L	lift force (N)
F_M	Magnus force (N)
F_S	Saffman force (N)
F_T	turbulence force (N)
g	acceleration due to gravity (m/s^2)
H	liquid height (m)
h	height of the calibration plate from the tank bottom (mm)
i	the distance of the horizontal plane from the bottom of the tank for LES data (mm)
L	integral length scale (m)
N	impeller rotational speed (rpm)
N_{expt}	impeller speed for the PIV experiments (rpm)
N_{js}	just suspended speed (rpm)
N_p	power number (dimensionless)
n	clearance index in Eq. (13)
P_{js}	power consumption at the just suspended speed (W)
R	radial position in the tank (mm)
S	Zwietering's N_{js} constant
T	tank diameter (m)
U	velocity in Eq. (3) (m/s)
U^*	shear velocity (m/s)
$V_{measured}$	measured velocity (m/s)
V_r	mean radial velocity (m/s)
V_{scaled}	scaled mean radial or axial rms velocity (m/s)
V_{tip}	tip velocity (m/s)
v'_z	axial rms velocity (m/s)
W	baffle width (m)
X	solids loading (mass of solid/mass of liquid $\times$ 100)
x	the length scale (m)
x_n	velocity at the nth off-bottom clearance
x_{mean}	the mean velocity over all six clearances
y	distance from the solid surface (m)
y^+	dimensionless distance from the solid surface

Greek characters

ν	kinematic viscosity of the liquid (m^2/s)
μ_L	dynamic viscosity of the liquid (kg/m s)
ρ_L	liquid density (kg/m^3)
ρ_S	solid density (kg/m^3)
ρ_{sl}	slurry density (kg/m^3)
σ	normalized standard deviation (Eq. (12))
$\Delta\sigma$	difference between the normalized standard deviations of the scaled and measured velocities (Eq. (13))
$\Delta\sigma_r$	$\Delta\sigma$ for mean radial velocities
$\Delta\sigma_z$	$\Delta\sigma$ for axial rms velocities
η	Kolmogoroff length scale
η_{est}	estimated Kolmogoroff length scale
ε	rate of dissipation of turbulent kinetic energy per unit mass (m^2/s^3)
δ	viscous sub-layer thickness (m)

Abbreviations

Ar	Archimedes number
A310	axial impeller provided by Lightnin
B	bronze
DNS	direct numerical simulations
LES	large eddy simulations
LG	large glass beads
min	minimum
max	maximum
PIV	particle image velocimetry
Re	Reynolds number
rms	root mean square
SG	small glass beads
wt%	weight percent

Acknowledgments

The authors would like to thank Lightnin, NSERC, and CNPq, Brazil, for funding this research.

References

Armenante, P.M., Nagamine, E.U., Susanto, J., 1998. Determination of correlations to predict the minimum agitation speed complete solid suspension in agitated vessels. Can. J. Chem. Eng. 76, 413–419.
Ayranci, I., Kresta, S.M., 2011. Design rules for suspending concentrated mixtures of solids in stirred tanks. Chem. Eng. Res. Des. 89, 1961–1971.
Baldi, G., Conti, R., Alaria, E., 1978. Complete suspension of particles in mechanically agitated vessels. Chem. Eng. Sci. 33, 21–25.
Bittorf, K.J., Kresta, S.M., 2003. Prediction of cloud height for solid suspension in stirred tanks. Trans. IChemE 81(A), 568–577.
Davies, J.T., 1972. Turbulence phenomena, an introduction to the eddy transfer of momentum, mass, and heat, particularly at interfaces. Academic Press, New York (chapter 3).
Derksen, J., Van den Akker, H.E.A., 1999. Large eddy simulations on the flow driven by a Rushton turbine. AICHE J. 45, 209–221.
Garcia, M.H., 2008. Sedimentation engineering: processes, management, modeling, and practice. Am. Soc. Civ. Eng., 21–306.
Ghionzoli, A., Bujalski, W., Grenville, R.K., Nienow, A.W., Sharpe, R.W., Paglianti, A., 2007. The effect of bottom roughness on the minimum agitator speed required to just fully suspend particles in a stirred vessel. Trans. IChemE 85 (A5), 685–690.
Grenville, R.K., Mak, A.T.C., Brown, D.A.R., 2010. An improved correlation to predict "just suspension" speed for solid–liquid mixtures with axial flow impellers in stirred tanks. North American Mixing Forum, Victoria, BC, Canada (June 20–June 25).
Kresta, S.M., Wood, P.E., 1993. The mean flow field produced by a 45° pitched blade turbine: changes in the circulation pattern due to off bottom clearance. Can. J. Chem. Eng. 71, 42–53.
Madej, A.M., Babazadeh, H., Nobes, D.S., 2011. The effect of chamber length and Reynolds number on jet precession. Exp. Fluid 51 (6), 1623–1643.
Molerus, O., Latzel, W., 1987. Suspension of solid particles in agitated vessels. Particulate Sci. Technol. 5 (3), 235–260.
Myers, K.J., Fasano, J.B., 1992. The influence of baffle off-bottom clearance on the solids suspension of pitched-blade and high-efficiency impellers. Can. J. Chem. Eng. 70, 596–599.
Nienow, A.W., 1968. Suspension of solid particles in turbine agitated baffled vessels. Chem. Eng. Sci. 23, 1453–1459.
Nouri, J.M., Whitelaw, J.H., Yianneskis, M., 1987. The scaling of the flow field with impeller size and rotational speed in a stirred reactor. In: Proceedings of the Second International Conference on Laser Anemometry—Advances and Applications. Strathclyde, UK.
Tatterson, G.B., Yuan, H.H.S., Brodkey, R.S., 1980. Stereoscopic visualization of the flows for pitched blade turbines. Chem. Eng. Sci. 35 (6), 1369–1375.
Thorpe, R.B., Stevenson, P., 2003. Suspension of particles from the bottom of pipes and stirred tanks by gassed and ungassed flows. Can. J. Chem. Eng. 81, 351–359.
Vanoni, V.A., 2006. Chapter II: Sediment Transportation Mechanics, Sedimentation Engineering. ASCE Manuals and Reports on Engineering Practice, second ed., vol. 54, pp. 11–189.
Wilson, K.C., 2005. Slurry transport using centrifugal pumps. Springer, New York, pp. 123–151.
Wilson, K.C., Sanders, R.S., Gillies, R.G., Shook, C.A., 2010. Verification of the near-wall model for slurry flow. Powder Technol. 197, 247–253.
Zhou, G., Kresta, S.M., 1996. Impact of tank geometry on the maximum turbulence energy dissipation rate for impellers. AICHE J. 42, 2476–2490.
Zwietering, Th.N., 1958. Suspending of solid particles in liquid by agitators. Chem. Eng. Sci. 8, 244–253.